ARL-RP-0526 ● JULY 2015

US Army Research Laboratory

Crystal Thermoelasticity at Extreme Loading Rates and Pressures: Analysis of Higher-Order Energy Potentials

by John D Clayton

A reprint from Extreme Mechanics Letters. 2015;3:113–122.

NOTICES (12 pt)

Disclaimers

The findings in this report are not to be construed as an official Department of the Army position unless so designated by other authorized documents.

Citation of manufacturer's or trade names does not constitute an official endorsement or approval of the use thereof.

Destroy this report when it is no longer needed. Do not return it to the originator.

ARL-RP-0526 ● JULY 2015

US Army Research Laboratory

Crystal Thermoelasticity at Extreme Loading Rates and Pressures: Analysis of Higher-Order Energy Potentials

by John D Clayton
Weapons and Materials Research Directorate, ARL

A reprint from Extreme Mechanics Letters. 2015;3:113–122.

REPORT DOCUMENTATION PAGE

Form Approved
OMB No. 0704-0188

1. REPORT DATE *(DD-MM-YYYY)*	2. REPORT TYPE	3. DATES COVERED (From - To)
July 2015	Reprint	1 March 2014–31 March 2015

4. TITLE AND SUBTITLE
Crystal Thermoelasticity at Extreme Loading Rates and Pressures: Analysis of Higher-Order Energy Potentials

5a. CONTRACT NUMBER

5b. GRANT NUMBER

5c. PROGRAM ELEMENT NUMBER

6. AUTHOR(S)
John D Clayton

5d. PROJECT NUMBER
DRI13-WMR019

5e. TASK NUMBER

5f. WORK UNIT NUMBER

7. PERFORMING ORGANIZATION NAME(S) AND ADDRESS(ES)
US Army Research Laboratory
ATTN: RDRL-WMP-C
Aberdeen Proving Ground, MD 21005-5069

8. PERFORMING ORGANIZATION REPORT NUMBER
ARL-RP-0526

9. SPONSORING/MONITORING AGENCY NAME(S) AND ADDRESS(ES)

10. SPONSOR/MONITOR'S ACRONYM(S)

11. SPONSOR/MONITOR'S REPORT NUMBER(S)

12. DISTRIBUTION/AVAILABILITY STATEMENT
Approved for public release; distribution is unlimited.

13. SUPPLEMENTARY NOTES
A reprint from Extreme Mechanics Letters. 2015;3:113–122.

14. ABSTRACT
Several finite elastic strain measures are evaluated for use in constitutive models of crystalline elasticity and elasto-plasticity. These include the Green material strain tensor, the Eulerian material strain tensor, and the logarithmic material strain tensor, all of which are referred to locally relaxed coordinates invariant under spatial rotations. New applications of logarithmic strain-based theory towards shock compression of aluminum, copper, and magnesium single crystals and polycrystals are presented. Solutions to the planar shock problem from previous work are summarized and compared with the present results. Consideration of these new results in conjunction with previous analysis for a number of different metals, ceramics, and minerals suggests that Eulerian strain-based theory is most accurate for modeling the dynamic high-pressure response of ductile metallic crystals wherein ratios of elastic shear to bulk moduli tend to be relatively small, while logarithmic strain-based theory is recommended for modeling shocks in ceramics and minerals with larger ratios of effective elastic shear to bulk modulus.

15. SUBJECT TERMS
dynamic loading, shock compression, constitutive modeling, nonlinear elasticity, equation of state

16. SECURITY CLASSIFICATION OF:			17. LIMITATION OF ABSTRACT	18. NUMBER OF PAGES	19a. NAME OF RESPONSIBLE PERSON
a. REPORT	b. ABSTRACT	c. THIS PAGE			John D Clayton
Unclassified	Unclassified	Unclassified	UU	16	19b. TELEPHONE NUMBER (Include area code) 410-278-6146

Extreme Mechanics Letters 3 (2015) 113–122

Contents lists available at ScienceDirect

Extreme Mechanics Letters

journal homepage: www.elsevier.com/locate/eml

Crystal thermoelasticity at extreme loading rates and pressures: Analysis of higher-order energy potentials

J.D. Clayton *

Impact Physics, US ARL, Aberdeen, MD 21005-5066, USA

ARTICLE INFO

Article history:
Received 20 November 2014
Received in revised form 23 February 2015
Accepted 12 March 2015
Available online 15 March 2015

Keywords:
Dynamic loading
Shock compression
Constitutive modeling
Nonlinear elasticity

ABSTRACT

Several finite elastic strain measures are evaluated for use in constitutive models of crystalline elasticity and elasto-plasticity. These include the Green material strain tensor, the Eulerian material strain tensor, and the logarithmic material strain tensor, all of which are referred to locally relaxed coordinates invariant under spatial rotations. New applications of logarithmic strain-based theory towards shock compression of aluminum, copper, and magnesium single crystals and polycrystals are presented. Solutions to the planar shock problem from previous work are summarized and compared with the present results. Consideration of these new results in conjunction with previous analysis for a number of different metals, ceramics, and minerals suggests that Eulerian strain-based theory is most accurate for modeling the dynamic high-pressure response of ductile metallic crystals wherein ratios of elastic shear to bulk moduli tend to be relatively small, while logarithmic strain-based theory is recommended for modeling shocks in ceramics and minerals with larger ratios of effective elastic shear to bulk modulus.

Published by Elsevier Ltd.

1. Introduction

The shock response of solids is important in applications related to structural crashworthiness, defense (e.g., projectile–target interactions), and geophysics (e.g., explosive mining operations and hypervelocity collisions of planetary rock masses) [1]. Accurate, efficient, stable, and thermodynamically consistent models for nonlinear anisotropic elasticity are required for proper mesoscale modeling of crystalline solids subjected to impact or ballistic loading. Nonlinear hyperelasticity addresses the thermodynamically reversible response component of solids subjected to large deformation; classes of crystalline materials of interest include metals [2], ceramics and minerals [3], energetic materials [4], and electronic materials [5].

This Letter considers three particular nonlinear thermoelasticity models–each based on a different finite strain tensor referred to locally unstressed material coordinates–and their performance regarding depiction of shock compression of crystalline solids. The three strain measures are the elastic Green–Lagrange strain $\boldsymbol{E}$ (often simply referred to here as Green strain), Eulerian material strain $\boldsymbol{D}$, and logarithmic material strain $\boldsymbol{e}$, all defined mathematically later in the text.

Conventional Lagrangian formulations of nonlinear elasticity for crystals [6,7] incorporate the elastic Green strain tensor. However, benefits of Eulerian strain tensors for isotropic materials were predicted [8] and demonstrated for cubic crystals under hydrostatic stress [9]. Thermal effects were considered in [10] for cubic crystals, and a theory for non-cubic crystals was initiated in [11]. A complete $\boldsymbol{D}$-based continuum thermoelastic theory for large deformation of crystals of arbitrary symmetry was developed in [12]. Analytical solutions for homogeneous deformations of ideal cubic crystals were studied over a prescribed range of elastic coefficients; stress states and

* Correspondence to: Adjunct Faculty, A. James Clark School of Engineering, University of Maryland, College Park, USA.
E-mail addresses: john.d.clayton1.civ@mail.mil, jdclayt1@umd.edu.

http://dx.doi.org/10.1016/j.eml.2015.03.005
2352-4316/Published by Elsevier Ltd.

intrinsic stability measures were compared. For realistic coefficients, Eulerian theory predicted more physically realistic and stable behavior than Lagrangian theory under large compression and shear. Analytical solutions for shock compression of anisotropic single crystals were derived for internal energy functions quartic in Lagrangian or Eulerian strain and linear in entropy; results were analyzed for nonmetals quartz, sapphire, and diamond in [12] and metals aluminum, copper, and magnesium in [13]. Eulerian theory was recently used to numerically model the viscoplastic response of aluminum single crystals and textured polycrystals in wave propagation simulated using the finite difference method [14], wherein Lagrangian theory was found insufficient for modeling strong/overdriven elastic–plastic shocks.

A complete $\boldsymbol{e}$-based continuum thermoelastic theory was analogously developed in [15] and applied to study the shock response of the same three nonmetals. The theory was extended to describe elastic–plastic response using a multiplicative decomposition of the deformation gradient (formally given later in Eq. (2)), and solutions for plastic shocks (involving slip, twinning, and/or shear fractures) following an elastic precursor in rate independent solids were derived [15]. Logarithmic theory delivered superior accuracy to Lagrangian and Eulerian theories for modeling shocks in single crystals of sapphire (X- and Z-cut), quartz (Z-cut), and diamond (X-cut) [15]. Logarithmic theory incorporating third-order elastic constants was also applied to analytically model the elastic–inelastic response of isotropic polycrystalline titanium diboride ceramic [16], including double yield and effects of static lateral pre-stress.

The remainder of this Letter is organized as follows. Kinematics and strain tensors are formally defined in Section 2, along with three-dimensional forms of internal energy functions. Specialization of the general theory to shock loading and large volumetric deformation is reviewed in Section 3. Analytical solutions corresponding to energy potentials associated with different strain tensors are compared with each other, experimental data, and atomic simulation data in Section 4, leading to suggested/preferred potentials for use in various situations. Conclusions follow in Section 5. Notation of continuum mechanics is used: vectors and tensors in bold font, scalars in italics, and summation over repeated indices (subscripts) referred to Cartesian coordinates. As befitting the brief style of a Letter, derivations that can be found in the cited references are usually omitted.

2. General constitutive theory

At a material element with reference coordinates $\boldsymbol{X}$ and spatial coordinates $\boldsymbol{x}$, the deformation gradient $\boldsymbol{F}$ and volume ratio J are

$$\begin{aligned} &\boldsymbol{F}(\boldsymbol{X}) = \partial \boldsymbol{x}/\partial \boldsymbol{X}, \\ &F_{ij}(X_K) = \partial x_i/\partial X_J = \delta_{ij} + \partial u_i/\partial X_J; \\ &J(\boldsymbol{X}) = V/V_0 = \det \boldsymbol{F}; \end{aligned} \tag{1}$$

where $\boldsymbol{u}$ is the particle displacement. For an elastic–plastic material, where "plastic" refers here to any thermodynamically irreversible mechanism such as dislocation glide, deformation twinning, fracture, void growth, or pore collapse, the total deformation gradient is typically split into a product of a thermoelastic term (superscript E) and a plastic term (superscript P, and which can be further decomposed into a product of deformation mappings associated with different physical mechanisms) [2–4,6,17]:

$$\begin{aligned} &\boldsymbol{F} = \boldsymbol{F}^E\boldsymbol{F}^P, \qquad F_{ij} = F^E_{iK}F^P_{Kj}; \\ &J = J^EJ^P = \det \boldsymbol{F}^E \det \boldsymbol{F}^P. \end{aligned} \tag{2}$$

The elastic Green material strain tensor (i.e., Green–Lagrange strain) is defined as [6,7]

$$\boldsymbol{E} = \frac{1}{2}(\boldsymbol{F}^{ET}\boldsymbol{F}^E - \boldsymbol{1}), \qquad E_{IJ} = \frac{1}{2}(F^E_{kI}F^E_{kJ} - \delta_{IJ}). \tag{3}$$

Also considered here are theories incorporating the elastic Eulerian material strain tensor [12–14]

$$\boldsymbol{D} = \frac{1}{2}(\boldsymbol{1} - \boldsymbol{F}^{E-1}\boldsymbol{F}^{E-T}), \qquad D_{ij} = \frac{1}{2}(\delta_{ij} - F^{E-1}_{Ik}F^{E-1}_{Jk}) \tag{4}$$

and the elastic material logarithmic strain tensor [15,16]

$$\begin{aligned} &\boldsymbol{e} = \ln \boldsymbol{U}^E = \frac{1}{2}\ln(\boldsymbol{F}^{ET}\boldsymbol{F}^E) = \frac{1}{2}\ln \boldsymbol{C}^E, \\ &e_{IJ} = \frac{1}{2}\ln(\boldsymbol{F}^{ET}\boldsymbol{F}^E)_{IJ}. \end{aligned} \tag{5}$$

Complete presentations of thermodynamic theories can be found in [12–16] and are too lengthy to reproduce in entirety in this Letter. Several important relations are listed next for reference. Local balance laws are, in the absence of discontinuities, body forces, and heat conduction,

$$\rho_0 = \rho J, \qquad \nabla \cdot \boldsymbol{\sigma} = \rho \ddot{\boldsymbol{x}}, \qquad \dot{U} = J\boldsymbol{\sigma} : (\dot{\boldsymbol{F}}\boldsymbol{F}^{-1}), \tag{6}$$

with ρ_0 and ρ reference and spatial mass densities, $\boldsymbol{\sigma}$ symmetric Cauchy stress, and U internal energy per reference volume. Letting ξ denote an internal state variable linked to evolution of microstructure (e.g., defects) and η the entropy density, forms of internal energy functions are

$$\begin{aligned} &U = \bar{U}(\boldsymbol{E}, \eta, \xi), \qquad U = \hat{U}(\boldsymbol{D}, \eta, \xi), \\ &U = \breve{U}(\boldsymbol{e}, \eta, \xi). \end{aligned} \tag{7}$$

Corresponding thermoelastic relationships for stress $\boldsymbol{\sigma}$ and temperature θ follow as [12,15]

$$\begin{aligned} &\boldsymbol{\sigma} = J^{E-1}\boldsymbol{F}^E(\partial \bar{U}/\partial \boldsymbol{E})\boldsymbol{F}^{ET}, \\ &\boldsymbol{\sigma} = J^{E-1}\boldsymbol{F}^{E-T}(\partial \hat{U}/\partial \boldsymbol{D})\boldsymbol{F}^{E-1}, \\ &\boldsymbol{\sigma} = J^{E-1}\boldsymbol{F}^E[(\partial \breve{U}/\partial \boldsymbol{e}) : (\partial \ln \boldsymbol{C}^E/\partial \boldsymbol{C}^E)]\boldsymbol{F}^{ET}; \end{aligned} \tag{8}$$

$$\theta = \partial \bar{U}/\partial \eta, \qquad \theta = \partial \hat{U}/\partial \eta, \qquad \theta = \partial \breve{U}/\partial \eta. \tag{9}$$

At fixed entropy and internal state variables, assuming a stress-free reference configuration, and written explicitly with elastic constants up to fourth order, internal energy

functions per unit reference volume are expressed as the Taylor polynomials

$$\bar{U}(\boldsymbol{E}) = \frac{1}{2!}\mathrm{C}_{\alpha\beta}E_\alpha E_\beta + \frac{1}{3!}\bar{\mathrm{C}}_{\alpha\beta\gamma}E_\alpha E_\beta E_\gamma + \frac{1}{4!}\bar{\mathrm{C}}_{\alpha\beta\gamma\delta}E_\alpha E_\beta E_\gamma E_\delta + \cdots, \tag{10}$$

$$\hat{U}(\boldsymbol{D}) = \frac{1}{2!}\mathrm{C}_{\alpha\beta}D_\alpha D_\beta + \frac{1}{3!}\hat{\mathrm{C}}_{\alpha\beta\gamma}D_\alpha D_\beta D_\gamma + \frac{1}{4!}\hat{\mathrm{C}}_{\alpha\beta\gamma\delta}D_\alpha D_\beta D_\gamma D_\delta + \cdots, \tag{11}$$

$$\breve{U}(\boldsymbol{e}) = \frac{1}{2!}\mathrm{C}_{\alpha\beta}e_\alpha e_\beta + \frac{1}{3!}\breve{\mathrm{C}}_{\alpha\beta\gamma}e_\alpha e_\beta e_\gamma + \frac{1}{4!}\breve{\mathrm{C}}_{\alpha\beta\gamma\delta}e_\alpha e_\beta e_\gamma e_\delta + \cdots. \tag{12}$$

Greek indices denote Voigt notation (e.g., $\alpha = 1, 2, \ldots, 6$). Elastic constant tensors of all orders have the same symmetries, though magnitudes of higher-order constants differ among the three representations. Consistent relationships among third-, and higher-order elastic constants have been derived elsewhere for various symmetry classes [9–16,18], allowing values of Lagrangian constants of potential energy in (10) to be converted to Eulerian and logarithmic analogs in (11) and (12) without the need for further material characterization experiments. Isentropic second-order elastic constants $\mathrm{C}_{\alpha\beta}$ are equal among all three theoretical representations in (10)–(12).

It is emphasized that all theories considered in the present paper are fully nonlinear; no considerations of nor comparisons with the usual linear theory of elasticity are included. Sources of nonlinearity are generally both geometric, arising from definitions of finite elastic strain measures in (3)–(5) for a given value of $\boldsymbol{F}^E$, and constitutive, arising from incorporation of nonzero higher-order elastic constants (cubic and higher-order terms) in (10)–(12). The nonlinear representations enable consideration of finite deformations, of particular interest large volume changes under compressive loading. However, when elastic displacement gradient components and relevant higher-order constants are sufficiently small in magnitude, results of all three representations collapse to those of anisotropic linear elasticity.

Axial components of the three strain tensors are compared for homogeneous spherical and uniaxial elastic deformations in Fig. 1. The magnitude of the axial component of $\boldsymbol{D}$ increases much more rapidly than that of $\boldsymbol{E}$ under compression, with $\boldsymbol{e}$ demonstrating trends intermediate to the other strains. Internal energy, stress/pressure, and bulk stiffness of crystals tend to increase rapidly with compression [19]. Therefore, Eulerian and logarithmic theories would be expected to converge faster, with fewer higher-order elastic constants needed, than Lagrangian theory, as will be verified later in this Letter.

3. Shock compression

New application of logarithmic strain-based theory ($\boldsymbol{e}$-based theory) to shock compression of metals is presented later in Section 4. These model predictions are thermoelastic and strictly applicable only for very small volumes,

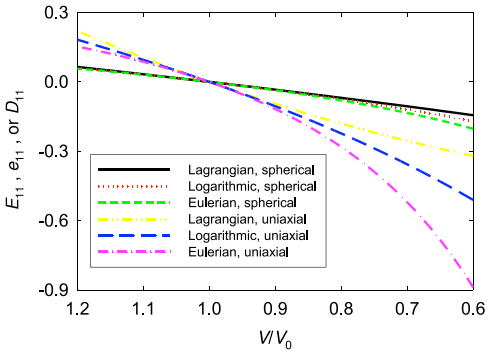

Fig. 1. Lagrangian (E_{11}), logarithmic (e_{11}), and Eulerian (D_{11}) strain in uniform deformation $J = V/V_0$. Spherical: $\boldsymbol{F} = J^{1/3}\boldsymbol{1}$; Uniaxial: $\boldsymbol{F} = \boldsymbol{1} + (J-1)\boldsymbol{e}_1 \otimes \boldsymbol{e}_1$.

such as in atomic simulations [20,21] or in the immediate vicinity of pinned defect cores [22], wherein plastic deformation does not occur. Let $X = X_1$ denote the direction of propagation of a purely longitudinal, steady thermoelastic shock wave of natural velocity $\mathcal{D}$ passing through a material initially unstressed and at rest. Since the shock is modeled as a jump discontinuity in axial particle velocity $v = \partial u(X,t)/\partial t$, the strain rate (velocity gradient) in the shock front tends towards infinity. Axial shock stress P is defined as positive in compression and is equal to the negative of Cauchy stress component σ_{11}. Solutions to this planar thermoelastic shock problem in anisotropic crystals were derived fully for Lagrangian and Eulerian theories in [12] and for logarithmic theory in [15]; the procedure involves simultaneous solution of Rankine–Hugoniot equations for conservation of mass, momentum, and energy:

$$\mathcal{D} = v/(1-J), \qquad P = \rho_0 \mathcal{D} v, \qquad U = \frac{1}{2}\rho_0 v^2 \tag{13}$$

along with consideration of internal energy functions (10), (11), or (12) of order four in corresponding strain and extended to include entropy change $\Delta\eta$ via Grunëisen tensor Γ_α:

$$\bar{U}(\boldsymbol{E},\eta) = \frac{1}{2}\mathrm{C}_{\alpha\beta}E_\alpha E_\beta + \frac{1}{6}\bar{\mathrm{C}}_{\alpha\beta\gamma}E_\alpha E_\beta E_\gamma + \frac{1}{24}\bar{\mathrm{C}}_{\alpha\beta\gamma\delta}E_\alpha E_\beta E_\gamma E_\delta + \theta_0\Delta\eta(1-\Gamma_\alpha E_\alpha), \tag{14}$$

$$\hat{U}(\boldsymbol{D},\eta) = \frac{1}{2}\mathrm{C}_{\alpha\beta}D_\alpha D_\beta + \frac{1}{6}\hat{\mathrm{C}}_{\alpha\beta\gamma}D_\alpha D_\beta D_\gamma + \frac{1}{24}\hat{\mathrm{C}}_{\alpha\beta\gamma\delta}D_\alpha D_\beta D_\gamma D_\delta + \theta_0\Delta\eta(1-\Gamma_\alpha D_\alpha), \tag{15}$$

$$\breve{U}(\boldsymbol{e},\eta) = \frac{1}{2}\mathrm{C}_{\alpha\beta}e_\alpha e_\beta + \frac{1}{6}\breve{\mathrm{C}}_{\alpha\beta\gamma}e_\alpha e_\beta e_\gamma + \frac{1}{24}\breve{\mathrm{C}}_{\alpha\beta\gamma\delta}e_\alpha e_\beta e_\gamma e_\delta + \theta_0\Delta\eta(1-\Gamma_\alpha e_\alpha). \tag{16}$$

The explicit analytical solutions for shock stress to order three in each of the uniaxial scalar strain measures ($E = E_{11}$, $D = D_{11}$, $e = e_{11}$) derived in full elsewhere [12,13,15]

are

$$P = -J\partial\bar{U}/\partial E = -J[\mathrm{C}_{11}E + \frac{1}{2}\bar{\mathrm{C}}_{111}E^2 + \frac{1}{6}(\bar{\mathrm{C}}_{1111} - A\theta_0\Gamma_1)E^3] \quad \text{(Lagrangian)}, \tag{17}$$

$$P = -J^{-3}\partial\hat{U}/\partial D = -J^{-3}[\mathrm{C}_{11}D + \frac{1}{2}\hat{\mathrm{C}}_{111}D^2 + \frac{1}{6}(\hat{\mathrm{C}}_{1111} - A\theta_0\Gamma_1)D^3] \quad \text{(Eulerian)}, \tag{18}$$

$$P = -J^{-1}\partial\breve{U}/\partial e = -J^{-1}[\mathrm{C}_{11}e + \frac{1}{2}\breve{\mathrm{C}}_{111}e^2 + \frac{1}{6}(\breve{\mathrm{C}}_{1111} - A\theta_0\Gamma_1)e^3] \quad \text{(Logarithmic)}, \tag{19}$$

where for uniaxial strain, with θ_0 the ambient temperature upstream from the shock:

$$J = (1+2E)^{1/2} = (1-2D)^{-1/2} = \exp(e),$$
$$2\theta_0 A = \bar{\mathrm{C}}_{111} + 3\mathrm{C}_{11} = \hat{\mathrm{C}}_{111} - 9\mathrm{C}_{11} = \breve{\mathrm{C}}_{111} - 3\mathrm{C}_{11}. \tag{20}$$

From (9) and (14)–(16), temperature in the shocked state is, for each theoretical representation,

$$\theta = \theta_0(1-\Gamma_1 E) \quad \text{(Lagrangian)};$$
$$\theta = \theta_0(1-\Gamma_1 D) \quad \text{(Eulerian)}; \tag{21}$$
$$\theta = \theta_0(1-\Gamma_1 e) \quad \text{(Logarithmic)}.$$

In these internal energy-based theories, effects of entropy production on stress arise from the rightmost terms proportional to A in each of (17)–(19), providing the increase in shock stress ΔP on the Hugoniot relative to that along a corresponding isentrope. Temperature rise does not explicitly enter (17)–(19), but its effects are implicit in the thermodynamic framework. For example, consider Eulerian theory with thermoelastic temperature rise $\Delta\theta = \theta - \theta_0$ given by the second of (21); dissipative stress increase relative to temperature rise then obeys $\Delta P = AD^2\Delta\theta/6$. Also, noting that isothermal second-order constants are related to isentropic constants via $\mathrm{C}^{\theta}_{\alpha\beta} = \mathrm{C}_{\alpha\beta} - \theta_0 c_0 \Gamma_\alpha \Gamma_\beta$ with c_0 specific heat at constant strain [6], isentropic constants tend to exceed their isothermal counterparts, leading to larger P for adiabatic relative to isothermal compression.

In laboratory scale specimens, yielding would commence in many pure ductile metals at small compressions at which effects of higher-order constants and differences among predictions from (17)–(19) would be negligible. However, nonlinear elastic effects on deviatoric stress may still be important at larger compressions after yielding, particularly for lower symmetry materials with restricted slip planes/directions [13], and the nonlinearity in pressure–volume response is important regardless of shear strength, as will become clear later in the context of results in Section 4.

When material strength (i.e., maximum sustained deviatoric stress) is low relative to mean stress and can safely be omitted, the response of metals to moderate shocks can often be adequately approximated ($p \approx P$) by an adiabatic pressure–volume (p–J) equation of state (EOS) derived for spherical compression, termed herein the hydrodynamic approximation. The EOS corresponding to each of (14)–(16) truncated at order three in strain is [12,13,15]

Table 1
Single crystal and polycrystal properties [13] ($\theta_0 = 295$ K; $\mathrm{C}_{\alpha\beta}$ in GPa; ρ_0 in g/cm^3).

Property	Al [100]	Cu [100]	Mg [a-axis]	Mg [c-axis]
C_{11}	107	166	59.4	61.6
$\bar{\mathrm{C}}_{111}$	−1080	−1279	−664	−728
$\hat{\mathrm{C}}_{111}$	203	715	49	12
$\breve{\mathrm{C}}_{111}$	−438	−283	−308	−358
$\bar{\mathrm{C}}_{1111}$	25 000	11 900	8170	7380
$\hat{\mathrm{C}}_{1111}$	10 500	2000	1220	893
$\breve{\mathrm{C}}_{1111}$	15 036	1200	1865	369
Γ_1	2.17	1.97	1.52	1.52
B_0	76	137	35.4	35.4
B'_0	4.42	5.48	3.90	3.90
ρ_0	2.70	8.96	1.74	1.74

$$p = -\partial\bar{U}/\partial J = \frac{3}{2}\mathrm{B}_0(J^{-1/3} - J^{1/3}) \times \left[1 - \frac{3}{4}\mathrm{B}'_0(J^{2/3} - 1)\right] \quad \text{(Lagrangian)}, \tag{22}$$

$$p = -\partial\hat{U}/\partial J = \frac{3}{2}\mathrm{B}_0(J^{-7/3} - J^{-5/3}) \times \left[1 + \frac{3}{4}(\mathrm{B}'_0 - 4)(J^{-2/3} - 1)\right] \quad \text{(Eulerian)}, \tag{23}$$

$$p = -\partial\breve{U}/\partial J = -\mathrm{B}_0[(\ln J)/J] \times \left[1 - \frac{1}{2}(\mathrm{B}'_0 - 2)\ln J\right] \quad \text{(Logarithmic)}, \tag{24}$$

where B_0 and B'_0 are isentropic bulk modulus and its pressure derivative in the unstressed reference state. Eulerian EOS (23) is equivalent to the Birch–Murnaghan EOS [9]. Appendix A gives requirements ensuring accuracy of this hydrodynamic approximation for shock loading.

4. Results and analysis

Thermoelastic and physical properties for aluminum (Al), copper (Cu), and magnesium (Mg) are reported in Table 1. Predictions for shock stress versus volume ratio are made using the analytical solutions of (17), (18), and (19), considering only pure mode directions of steady shock propagation (i.e., a strictly longitudinal response, with no transverse waves). Shock stress P normalized by second-order isentropic elastic constant C_{11} is shown in Fig. 2(a) for Al, Fig. 2(b) for Cu, Fig. 2(c) for Mg shocked along the [a-axis] and Fig. 2(d) for Mg shocked along the [c-axis]. Cubic crystals Al and Cu are shocked along [100] directions.

Higher-order elastic constants for Eulerian and logarithmic representations are converted from measured Lagrangian constants using formulae derived or presented in [12,13,15,18] and listed in Appendix B. Elastic constants of up to order four are considered in results labeled "4th order". Results labeled "3rd order" and "2nd order" are obtained, respectively, by setting fourth-order and both third- and fourth-order elastic constants to zero in (17)–(19). Results in Fig. 2 compare logarithmic and Eulerian

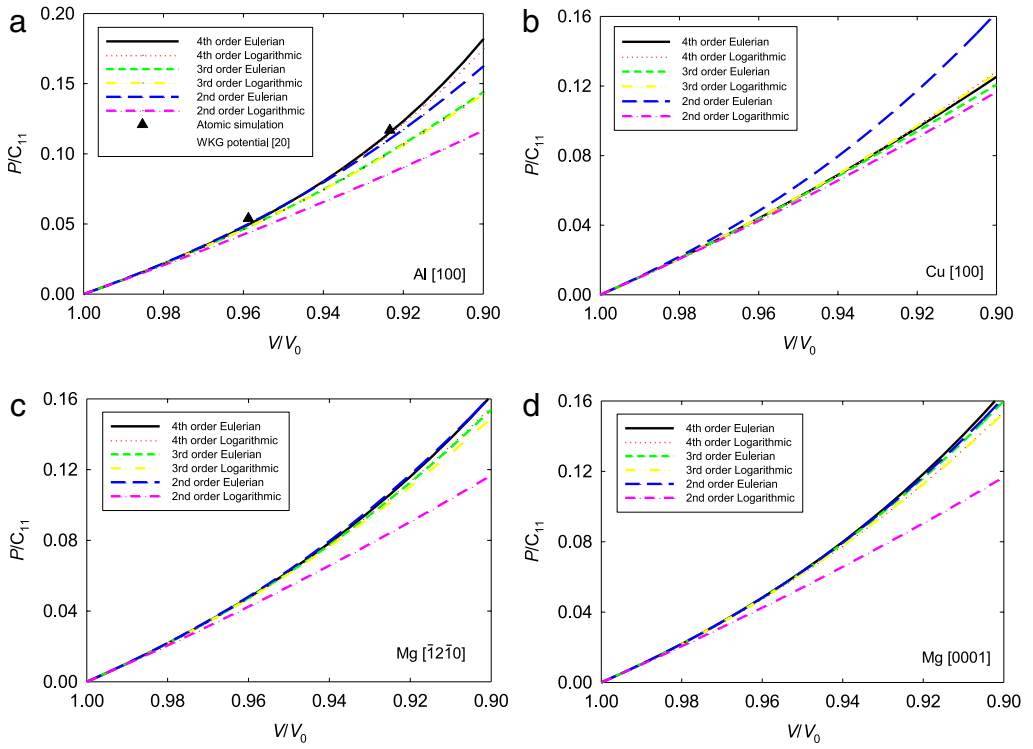

Fig. 2. Analytical anisotropic thermoelastic solutions for axial stress in (a) shocked aluminum (Al) single crystal along [100] compared with atomic simulation data [20], (b) shocked copper (Cu) single crystal along [100], (c) shocked magnesium (Mg) single crystal along *a*-axis, and (d) shocked Mg single crystal along *c*-axis.

Table 2
Relative difference Δ (%) in shock stress *P* predicted by 3rd (Lag3, Log3, Eul3) and 2nd (Lag2, Log2, Eul2) order theories: Al and Cu.

V/V_0	Aluminum [100]						Copper [100]					
	Lag3	Log3	Eul3	Lag2	Log2	Eul2	Lag3	Log3	Eul3	Lag2	Log2	Eul2
0.96	−5.0	−3.8	−3.1	−23.1	−11.9	+1.1	−1.6	−0.2	−0.4	−15.8	−3.7	+9.3
0.92	−15.7	−13.9	−14.1	−48.2	−29.8	−5.0	−5.4	−0.8	−2.1	−31.6	−7.8	+19.9
0.88	−28.1	−28.2	−34.5	−71.2	−51.0	−19.8	−10.4	−1.8	−6.2	−46.5	−12.4	+31.5

Table 3
Relative difference Δ in shock stress *P* predicted by 3rd (Lag3, Log3, Eul3) and 2nd (Lag2, Log2, Eul2) order theories: Mg.

V/V_0	Magnesium [*a*-axis]						Magnesium [*c*-axis]					
	Lag3	Log3	Eul3	Lag2	Log2	Eul2	Lag3	Log3	Eul3	Lag2	Log2	Eul2
0.96	−2.9	−0.8	−0.6	−22.8	−10.9	1.2	−2.5	−0.2	−0.4	−23.4	−11.0	−0.0
0.92	−9.2	−3.0	−2.9	−44.7	−22.7	1.0	−7.9	−0.6	−2.0	−45.1	−22.5	−1.2
0.88	−16.8	−6.3	−7.6	−64.3	−35.0	−1.4	−14.5	−1.2	−5.2	−64.2	−33.0	−3.8

theories; different plots comparing Lagrangian and Eulerian theories can be found in [13]. All longitudinal higher-order elastic constants (i.e., all third- and fourth-order constants) are smaller in magnitude for Eulerian and logarithmic theory than Lagrangian theory for these metals, as can be verified via examination of values in Table 1.

Stress predictions of 2nd and 3rd order models are usually closer to those of 4th order theory for Eulerian and logarithmic theory than for Lagrangian theory. Tables 2 and 3 list relative differences (%) of 2nd and 3rd order predictions compared to 4th order predictions, computed as

$$\Delta = 2 \cdot (\text{2nd or 3rd order result} - \text{4th order result}) / (\text{2nd or 3rd order result} + \text{4th order result}). \quad (25)$$

For each crystal type, such differences are almost always smaller in magnitude for Eulerian theory (Eul2, Eul3) and logarithmic theory (Log2, Log3) than for Lagrangian theory (Lag2, Lag3) at a given volume ratio and order of approximation, i.e., order of Taylor polynomial used in internal energy functions (14)–(16). If 4th order results are viewed as exact, then Δ can be interpreted as a measure of error of the lower order predictions; however, the term "error" is avoided in the present context since even the 4th order predictions may be subject to inaccuracy relative to "exact" polynomial representations containing up to an

infinite number of terms or relative to experimental data used for model validation.

These observations imply a faster converging series in (19) or (18) than (17) as the number of higher-order constants is increased and presumably greater accuracy of Eulerian or logarithmic theory than Lagrangian theory when the same number of constants (i.e., the same order of Taylor polynomial) is used in each representation. Eulerian and logarithmic theories trend towards comparable accuracy, with one theory or the other possibly more accurate for a given metal or order of approximation. For Al, as shown in Fig. 2(a), the analytical solution incorporating 4th order Eulerian theory best matches atomic predictions [20]. For example, at a compression ratio of $J = V/V_0 = 0.923$, the difference in 4th order Eulerian theory versus atomic simulation is −1.4%, compared to −7.4% for 4th order Lagrangian theory and −2.2% for 4th order logarithmic theory.

Comparison with results of empirical potential-based molecular dynamics (MD) calculations [20] may be viewed with some reservation since MD results are subject to their own possible sources of inaccuracy, e.g., uncertainty in assumed functional forms and parameters of the potentials and precision of numerical solutions. However, results of the Winey–Kubota–Gupta (WKG) potential considered in Fig. 2(a), first developed in [21], were reported in [20] to be more suitable than those of several other embedded atom-type potentials for modeling the uniaxial shock response of defect-free aluminum single crystals and in [21] more accurate for modeling thermoelasticity in Al over a wide temperature range. Furthermore, later in this paper, predictions of the nonlinear continuum models are compared directly with data from shock experiments and density functional theory (DFT) calculations (e.g., labeled as "ab initio", "first principles", "electronic structure" or "quantum-MD"), the latter typically viewed as less empirical than classical MD calculations, though again various assumptions and sources of inaccuracy are involved in solution of the governing quantum-mechanical relations [7].

Predicted shock stress P need not always increase (or decrease) as the order of approximation used in any of (17)–(19) is increased. Under uniaxial compression, finite strain measures E, D, and e are all negative in sign, leading to compressive (positive) contributions to P from positive second-order constants, tensile (negative) contributions to P from positive third-order constants, and compressive (positive) contributions to P from positive fourth-order constants. Signs of these contributions are reversed when signs of elastic constants are negative. For materials and properties of Table 1, all second- and fourth-order elastic constants are positive; third-order constants are all negative for Lagrangian and logarithmic theory and are all positive for Eulerian theory. As a result, predictions for logarithmic theory in Fig. 2 increase monotonically with increasing order, while predictions of Eulerian theory do not, with the 3rd order Eulerian prediction of P smaller than that of the 2nd order Eulerian prediction. As a general implication with regard to arbitrary materials, both the sign and magnitude of higher-order elastic constants should be considered when interpreting their importance in the context of stress predictions.

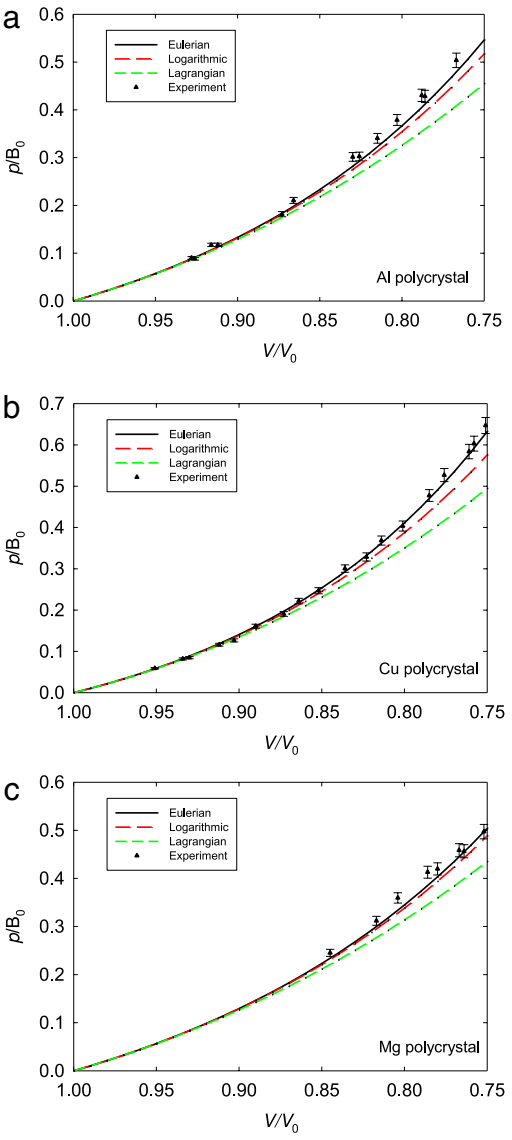

Fig. 3. Analytical solutions for polycrystalline (a) aluminum, (b) copper, and (c) magnesium in the hydrodynamic limit and experimental data [23].

Removing prior stated restrictions to defect-free or small volumes of single crystals, predictions of each third-order EOS in (22)–(24) are compared with polycrystalline shock compression data compiled in [23] for Al in Fig. 3(a), Cu in Fig. 3(b), and Mg in Fig. 3(c). Compressibility properties of Table 1 used in these predictions are obtained from ultrasonic experiments [24] and are not fit to the shock data.

Individual references from which experimental data are complied include [25–27] for Al, [25,28] for Cu, and [26] for Mg. Experimental methods, as discussed in detail in [25–29], involve measurements of shock wave velocity and in some cases free surface velocity for a specimen subjected to a planar shock generated by detonation in a high explosive system. Maximum uncertainties in volume change at fixed Hugoniot stresses as reported in these works range

from ±0.5% to ±2% [25–29]. Error bars on p/B_0 at fixed V are reasonably translated to ±3% in Fig. 3.

Relevance of the hydrodynamic assumptions detailed in Appendix A follows from the relatively low dynamic yield strength Y of these high purity metals, with values on the order of tens to several hundred MPa for dislocation glide in Al [14,18] and Cu [18,29] and for slip or twinning in Mg [30–32]. At very high rates, although Y may increase with pressure or decrease with thermal softening and shear localization, it follows that for $V/V_0 < 0.95$, $p/B_0 > 0.05$ in Fig. 3 and $Y/B_0 \approx O(10^{-3})$, leading to $Y/p < 0.02 \ll 1$ for each metal in these regimes of interest. The metallic polycrystals are effectively isotropic and plastically incompressible (i.e., non-porous). Hydrodynamic approximations were also found accurate for shocked Al and Cu in other works [18,29,33].

In each part of Fig. 3, Eulerian theory is most accurate, followed by logarithmic theory and then Lagrangian theory, with the latter much too compliant. Because Eulerian theory appears superior for modeling spherical compression and at least equally valid as logarithmic theory for modeling uniaxial strain compression, Eulerian theory is herein deemed preferable overall for representing the shock response of ductile metals.

As demonstrated in Appendix C, Eulerian theory also compares favorably with DFT results for static isothermal compression of Al, Cu, and Mg, especially with regard to relative accuracy of lower-order EOS predictions. Future numerical studies should thus consider applying Eulerian theory in finite element or finite difference simulations of the response of ductile metals, offering potential improvement over prior implementations incorporating Lagrangian theory [34–36].

On the other hand, recent work [15] found that logarithmic theory, while more computationally cumbersome than Eulerian theory, more accurately captures the shock response of ceramic crystals sapphire (α-Al_2O_3), diamond (C), and quartz (α-SiO_2), requiring fewer higher-order elastic constants to attain close agreement with experimental plate impact data. As shown in Table 4, these nonmetals have a large ratio of effective shear (G_0) to bulk modulus compared to metals, characteristic of the trend that G_0/B_0 tends to increase with brittleness in pure substances [37–39]. This correlation between plastic malleability and decreasing $G_0/B_0 = 3(1-2\nu)/(2+2\nu)$, first proposed by Pugh [37], is explained in terms of atomic structure and bonding in [38] and verified in the context of indentation hardness in [39]. Generally, resistance to bending of atomic bonds is reflected by the shear modulus, and resistance to stretching or compression of atomic bonds by the bulk modulus [38]. Second-order elastic constants can be related to harmonic interatomic forces, whereas higher-order constants depend on anharmonicity [40]. Future numerical studies of deformation of rock such as granite [41] (silicate minerals) should benefit from use of logarithmic rather than Lagrangian nonlinear elasticity.

Since the nonmetals considered in Table 4 tend to have a rather large Hugoniot Elastic Limit (HEL) (e.g., not occurring until up to ≈10% compression) and may demonstrate significant shear strength when shocked above their HEL [12], use of a pressure–volume EOS alone is insufficient for calculation of axial shock stress. However, suitability of logarithmic EOS (24) for representing the hydrostatic pressure–volume response has been verified for alumina, diamond, and quartz in [15]. Table 5 summarizes loading conditions, materials, and model performance studied in the present work (*) as well as results in [12,13,15]. In summary, Eulerian nonlinear theory is recommended for modeling the response of ductile metals, while logarithmic theory is recommended for modeling ceramics and minerals with larger ratios of shear to bulk stiffness.

Table 4
Ratio of ambient Voigt-averaged shear modulus to bulk modulus [13,15].

	Cu	Al	Mg	α-Al_2O_3	C	α-SiO_2
G_0/B_0	0.34	0.35	0.53	0.65	1.22	1.27

New contributions of the present paper are clarified as follows. Complete thermomechanical theories incorporating Eulerian and logarithmic strain measures were formalized in prior work [12–15]; the present paper contains new results and comparisons of applications of such theories for three metals (Al, Cu, and Mg) subjected to uniaxial shock compression (single crystals) and volumetric compression (polycrystals). In particular, predictions of Eulerian and logarithmic theories for these metals had not been compared previously with respect to order of representation, experimental data, or atomic simulation data (neither MD nor DFT). Such new comparisons, when viewed in conjunction with elastic constants listed in Table 4 and prior results listed in Table 5, have enabled discovery of a new inverse correlation between Pugh's ductility ratio [27] and suitability of Eulerian versus logarithmic theory for modeling shock compression processes, with the former preferred for lower values of the ratio G_0/B_0.

5. Conclusions

Constitutive theories and analytical solutions for thermoelastic compression relevant to shock loading (extreme strain rates and pressures) have been presented. Theories consider Taylor-type polynomial representations of internal energy density in one of three finite strain measures referred to unstressed material coordinates: Green strain, Eulerian strain, or logarithmic strain. The present results, newly examined in conjunction with prior work, imply that Eulerian theory should offer the greatest accuracy (at fixed order of Taylor polynomial) for modeling the shock response of typical ductile metals. In contrast, logarithmic theory is implied as most accurate for representation of the shock response of more brittle ceramics and minerals characterized by a relatively larger ratio of effective elastic shear modulus to bulk modulus in the initial state.

Appendix A. Hydrodynamic approximation

For the hydrodynamic approximation invoked implicitly in application of EOS calculations to shock response,

Table 5
Summary of present (*) and prior research results: finite strain model evaluations.

Loading Protocol	Material	Recommended theory	Remarks	Ref.
Hydrostatic compression	Ideal cubic, $B_0' = 4$	Eulerian	Eulerian more accurate p–V curves	[12]
Uniaxial compression	Ideal cubic, $B_0' = 4$	Eulerian	Eulerian more accurate and stable	[12]
Simple shear	Ideal cubic, $B_0' = 4$	Eulerian	Eulerian more accurate and stable	[12]
Shock compression	Sapphire (Al_2O_3)	Logarithmic	Logarithmic more accurate overall	[15]
Shock compression	Diamond (C)	Logarithmic	Logarithmic more accurate overall	[15]
Shock compression	α-Quartz (SiO_2)	Logarithmic	Logarithmic more accurate (Z-cut)	[12,15]
Shock compression	Aluminum (Al)	Eulerian	Eulerian best fit to atomic data	[13, *]
Shock compression	Copper (Cu)	Eulerian	Eulerian faster convergence	[13, *]
Shock compression	Magnesium (Mg)	Eulerian	Eulerian faster convergence	[13, *]
Shock compression	Al polycrystal	Eulerian	Eulerian more accurate	[*]
Shock compression	Cu polycrystal	Eulerian	Eulerian more accurate	[*]
Shock compression	Mg polycrystal	Eulerian	Eulerian more accurate	[*]

deviatoric stresses are assumed negligible relative to hydrostatic stress:

$$\boldsymbol{\sigma} \approx -p\mathbf{1} \Rightarrow \sigma_{11} \approx \sigma_{22} \approx \sigma_{33} \approx -p \\ \Rightarrow P = -\sigma_{11} \approx p. \tag{A.1}$$

Contributions from stress to internal energy in the third of (6) and (13) arise only from pressure:

$$\dot{U} = J\boldsymbol{\sigma} : \nabla \boldsymbol{v} = -Jp\nabla \cdot \boldsymbol{v} = -p\dot{J}, \\ p = -\partial U/\partial J = -V_0 \partial U/\partial V, \tag{A.2}$$

where plastic volume change has been assumed negligible in the second of (A.2) such that $J = J^E$. Total deformation need not be spherical in (A.2), but only volume changes perform mechanical work. Use of (A.1), (A.2) and (B.3) in (14)–(16) yields the EOS representations in (22)–(24). Use of (9) in (14)–(16) with $3\Gamma_0 = \mathrm{tr}\boldsymbol{\Gamma}$ yields the temperature rise resulting from a volume change:

$$\theta = \theta_0 \left[1 + \frac{3}{2}\Gamma_0(1 - J^{2/3})\right] \quad \text{(Lagrangian)}; \\ \theta = \theta_0 \left[1 + \frac{3}{2}\Gamma_0(J^{-2/3} - 1)\right] \quad \text{(Eulerian)}; \\ \theta = \theta_0[1 - \Gamma_0 \ln J] \quad \text{(Logarithmic)}. \tag{A.3}$$

The following modeling assumptions are inherent in the above derivations and the current application of (22)–(24) to describe planar shock compression processes in ductile metals:

- Deviatoric stress components are negligible relative to pressure; since such components are on the order of dynamic yield stress Y for metals [29], this translates to $Y/p \ll 1$;
- Entropy contributions to U can be adequately represented by rightmost linear terms in (14)–(16); this requires that magnitudes of entropy increases across the shock are modest, which is in accord with the first approximation above since plastic work contributions to entropy rise are correspondingly small when deviatoric stresses are sufficiently small;
- Other possible sources of internal energy change such as resulting from heat conduction, defect generation (ξ), and plastic volume change (J^P) are negligible; the first is in accord with usual adiabatic assumptions inherent in (6) and (13), the last in accord with usual kinematic descriptions that plastic deformation due to slip and twinning are isochoric;
- The material possesses cubic or isotropic elastic symmetry for (B.3) to hold, with isotropy applicable to polycrystalline metallic samples with many randomly oriented grains;
- Contributions of fourth- and higher-order in elastic strain to U (and thus orders three and higher to P) can be omitted, which in turn leads to omissions of higher-order derivatives such as B_0'' and A in each EOS in (22)–(24). Adequacy of this truncation can only be judged via accuracy of predictions of P or p, e.g., with experimental data.

Only the first of the above five points is mandatory for any general "hydrodynamic theory" that neglects material rigidity [25].

Appendix B. Higher-order elastic constants

Relationships among higher-order elastic constants entering Lagrangian, Eulerian, and logarithmic representations have been derived in several ways, including matching terms of strain energy potentials of equivalent powers [11,18], matching of tangent elastic moduli [12], and use of known formulae for derivatives of proper symmetric fourth-order tensor functions [42]. Consistent results from all methods of derivation for third-order longitudinal constants for a stress-free reference configuration are [11–13,18,42]

$$\bar{C}_{111} = \hat{C}_{111} - 12C_{11} = \breve{C}_{111} - 6C_{11}. \tag{B.1}$$

For fourth-order longitudinal elastic constants [13,18],

$$\bar{C}_{1111} = \hat{C}_{111} + 18\bar{C}_{111} + 318C_{11} \\ = \breve{C}_{1111} - 12\bar{C}_{111} - 28C_{11}. \tag{B.2}$$

The first pressure derivative of the bulk modulus at the reference state, for crystals of cubic or isotropic symmetry, with $3B_0 = C_{11} + 2C_{12}$ obeys [6,12,13,15,16]

$$B_0' = -\left(\frac{1}{9}\bar{C}_{111} + \frac{2}{3}\bar{C}_{112} + \frac{2}{9}\bar{C}_{123}\right) \Big/ B_0 \\ = -\left(\frac{1}{9}\hat{C}_{111} + \frac{2}{3}\hat{C}_{112} + \frac{2}{9}\hat{C}_{123}\right) \Big/ B_0 + 4 \\ = -\left(\frac{1}{9}\breve{C}_{111} + \frac{2}{3}\breve{C}_{112} + \frac{2}{9}\breve{C}_{123}\right) \Big/ B_0 + 2. \tag{B.3}$$

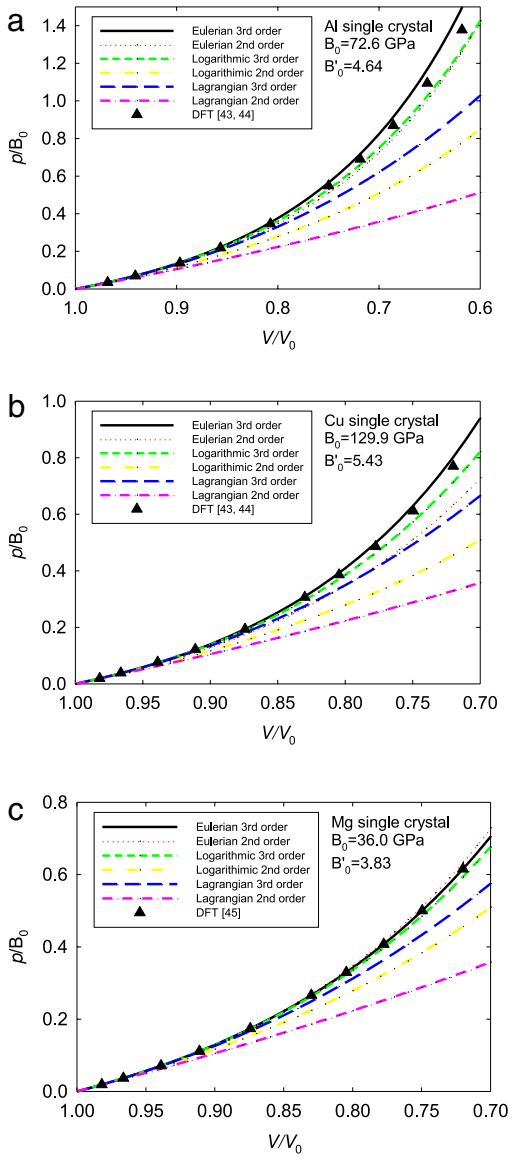

Fig. 4. Analytical EOS solutions and DFT data [43–45] for pure single crystalline (a) aluminum, (b) copper (c) magnesium.

Appendix C. Comparison with static DFT pressure–volume data

Predictions of each EOS in (22)–(24) are compared with isothermal compression data obtained from DFT calculations reported in [43–45] for pressures up to 100 GPa. Results for Al and Cu (FCC phases) correspond to room temperature (293 K) [43,44]; for Mg (HCP phase) to 0 K [45]. For proper comparison, isothermal values of bulk modulus and its pressure derivative as reported from the DFT works for each type of perfect single crystal are used in each EOS rather than isentropic polycrystalline values given previously in Table 1. Specifically, continuum EOS predictions labeled "3rd order" invoke values of B_0 and B_0' shown in the inset of each part of Fig. 4. Continuum EOS predictions labeled "2nd order" correspond to omission, in each EOS, of terms involving third-order elastic constants in (B.3), implying values of zero, two, and four for B_0' in (22), (24), and (23), respectively, noting, however, that (B.3) does not strictly apply for single crystal Mg with hexagonal symmetry.

As shown in Fig. 4, 3rd order Eulerian and logarithmic theories are of comparable accuracy relative to DFT data for Al, Cu, and Mg, with 3rd order Lagrangian theory less accurate (e.g., too compliant) at volume ratios J less than ≈0.85. Second-order logarithmic theory is too compliant for each material at volume ratios less than ≈0.90, and 2nd order Lagrangian theory is even more so, with the lowest relative accuracy among the three theories for the present application. However, 2nd order Eulerian theory is of comparable accuracy to 3rd order Eulerian and to 3rd order logarithmic theory for Al and Mg (Fig. 4(a) and (c)) and is more accurate than the two other 2nd order continuum elasticity predictions for Cu (Fig. 4(b)). In summary, Fig. 4 further supports the present recommendation for preferred use of Eulerian elasticity for modeling the high pressure response of ductile metals.

References

[1] A.K. Zurek, M.A. Meyers, Microstructural aspects of dynamic failure, in: L. Davison, D.E. Grady, M. Shahinpoor (Eds.), High-Pressure Shock Compression of Solids II, Springer, New York, 1996.
[2] R.A. Regueiro, D.J. Bammann, E.B. Marin, G.C. Johnson, Finite deformation elastoplasticity for rate and temperature dependent polycrystalline metals, in: Proceedings of ASME International Congress and Exposition IMECE 2011, American Society of Mechanical Engineers, Denver, 2011, pp. 111–123.
[3] J.D. Clayton, A continuum description of nonlinear elasticity, slip and twinning, with application to sapphire, Proc. R. Soc. Lond. Ser. A 465 (2009) 307–334.
[4] S. De, A.R. Zamiri, Rahul, A fully anisotropic single crystal model for high strain rate loading conditions with an application to α-RDX, J. Mech. Phys. Solids 64 (2014) 287–301.
[5] R. Zhu, E. Pan, P.W. Chung, X. Cai, K.M. Liew, A. Buldum, Atomistic calculation of elastic moduli in strained silicon, Semicond. Sci. Technol. 21 (2006) 906–911.
[6] J.D. Clayton, Nonlinear Mechanics of Crystals, Springer, Dordrecht, 2011.
[7] D.C. Wallace, Statistical Physics of Crystals and Liquids: a Guide to Highly Accurate Equations of State, World Scientific, Singapore, 2003.
[8] F.D. Murnaghan, Finite deformations of an elastic solid, Amer. J. Math. 59 (1937) 235–260.
[9] F. Birch, Finite elastic strain of cubic crystals, Phys. Rev. 71 (1947) 809–824.
[10] G.F. Davies, Effective elastic moduli under hydrostatic stress—I quasi-harmonic theory, J. Phys. Chem. Solids 35 (1974) 1513–1520.
[11] J.S. Weaver, Application of finite strain theory to non-cubic crystals, J. Phys. Chem. Solids 37 (1976) 711–718.
[12] J.D. Clayton, Nonlinear Eulerian thermoelasticity for anisotropic crystals, J. Mech. Phys. Solids 61 (2013) 1983–2014.
[13] J.D. Clayton, Shock compression of metal crystals: a comparison of Eulerian and Lagrangian elastic–plastic theories, Int. J. Appl. Mech. 6 (2014) 1450048.
[14] J.T. Lloyd, J.D. Clayton, R. Becker, D.L. McDowell, Simulation of shock wave propagation in single crystal and polycrystalline aluminum, Int. J. Plast. 60 (2014) 118–144.
[15] J.D. Clayton, Analysis of shock compression of strong single crystals with logarithmic thermoelastic–plastic theory, Internat. J. Engrg. Sci. 79 (2014) 1–20.
[16] J.D. Clayton, Finite strain analysis of shock compression of brittle solids applied to titanium diboride, Int. J. Impact Eng. 73 (2014) 56–65.
[17] K.N. Solanki, D.J. Bammann, A thermodynamic framework for a gradient theory of continuum damage, Acta Mech. 213 (2010) 27–38.
[18] G. Perrin, M. Delannoy-Coutris, Analysis of plane elastic–plastic shock-waves from the fourth-order anharmonic theory, Mech. Mater. 2 (1983) 139–153.

[19] R. Jeanloz, Shock wave equation of state and finite strain theory, J. Geophys. Res. 94 (1989) 5873–5886.
[20] J.A. Zimmerman, J.M. Winey, Y.M. Gupta, Elastic anisotropy of shocked aluminum single crystals: use of molecular dynamics simulations, Phys. Rev. B 83 (2011) 184113.
[21] J.M. Winey, A. Kubota, Y.M. Gupta, A thermodynamic approach to determine accurate potentials for molecular dynamics simulations: thermoelastic response of aluminum, Modelling Simul. Mater. Sci. Eng. 17 (2009) 055004.
[22] J.D. Clayton, Defects in nonlinear elastic crystals: differential geometry, finite kinematics, and second-order analytical solutions, Z. Angew. Math. Mech. (ZAMM) (2013) http://dx.doi.org/10.1002/zamm.201300142.
[23] S.P. Marsh, LASL Shock Hugoniot Data, University of California Press, Berkeley, 1980.
[24] M.W. Guinan, D.J. Steinberg, Pressure and temperature derivatives of the isotropic polycrystalline shear modulus for 65 elements, J. Phys. Chem. Solids 35 (1974) 1501–1512.
[25] J.M. Walsh, R.H. Christian, Equation of state of metals from shock wave measurements, Phys. Rev. 97 (1955) 1544–1556.
[26] J.M. Walsh, M.H. Rice, R.G. McQueen, F.L. Yarger, Shock-wave compressions of twenty-seven metals. Equations of state of metals, Phys. Rev. 108 (1957) 196–216.
[27] R.H. Warnes, Shock wave compression of three polynuclear aromatic compounds, J. Chem. Phys. 53 (1970) 1088–1094.
[28] R.G. McQueen, S.P. Marsh, Equation of state for nineteen metallic elements from shock-wave measurements to two megabars, J. Appl. Phys. 31 (1960) 1253–1269.
[29] H.K. Mao, P.M. Bell, J.W. Shaner, D.J. Steinberg, Specific volume measurements of Cu, Mo, Pd, and Ag and calibration of the ruby R1 fluorescence pressure gauge from 0.06 to 1 Mbar, J. Appl. Phys. 49 (1978) 3276–3283.
[30] P.D. Wu, H. Wang, K.W. Neale, On the large strain torsion of HCP polycrystals, Int. J. Appl. Mech. 4 (2012) 1250024.
[31] J.D. Clayton, J. Knap, A phase field model of deformation twinning: nonlinear theory and numerical simulations, Physica D 240 (2011) 841–858.
[32] J.D. Clayton, J. Knap, Phase-field analysis of fracture-induced twinning in single crystals, Acta Mater. 61 (2013) 5341–5353.
[33] R.G. Greene, H. Luo, A.L. Ruoff, Al as a simple solid: high pressure study to 220 GPa (2.2 Mbar), Phys. Rev. Lett. 73 (1994) 2075–2078.
[34] J.D. Clayton, D.L. McDowell, A multiscale multiplicative decomposition for elastoplasticity of polycrystals, Int. J. Plast. 19 (2003) 1401–1444.
[35] J.D. Clayton, Dynamic plasticity and fracture in high density polycrystals: constitutive modeling and numerical simulation, J. Mech. Phys. Solids 53 (2005) 261–301.
[36] J.D. Clayton, Modeling dynamic plasticity and spall fracture in high density polycrystalline alloys, Internat. J. Solids Structures 42 (2005) 4613–4640.
[37] S.F. Pugh, Relations between the elastic moduli and the plastic properties of polycrystalline pure metals, Phil. Mag. 45 (1954) 823–843.
[38] J.J. Gilman, Electronic Basis of the Strength of Materials, Cambridge University Press, Cambridge, 2003.
[39] X.-Q. Chen, H. Niu, D. Li, Y. Li, Modeling hardness of polycrystalline materials and bulk metallic glasses, Intermetallics 19 (2011) 1275–1281.
[40] J.D. Clayton, D.J. Bammann, Finite deformations and internal forces in elastic–plastic crystals: interpretations from nonlinear elasticity and anharmonic lattice statics, J. Eng. Mater. Technol. 131 (2009) 041201.
[41] J.D. Clayton, Deformation, fracture, and fragmentation in brittle geologic solids, Int. J. Fract. 163 (2010) 151–172.
[42] P. Dluzewski, Anisotropic hyperelasticity based on general strain measures, J. Elasticity 60 (2000) 119–129.
[43] Y. Wang, D. Chen, X. Zhang, Calculated equation of state of Al, Cu, Ta, Mo, and W to 1000 GPa, Phys. Rev. Lett. 84 (2000) 3220–3223.
[44] A. Dewaele, P. Loubeyre, M. Mezouar, Equations of state of six metals above 94 GPa, Phys. Rev. B 70 (2004) 094112.
[45] Q. Liu, C. Fan, R. Zhang, First-principles study of high-pressure structural phase transitions of magnesium, J. Appl. Phys. 105 (2009) 123505.

1 (PDF) DEFENSE TECHNICAL INFORMATION CTR DTIC OCA

2 (PDF) DIRECTOR US ARMY RESEARCH LAB RDRL CIO LL IMAL HRA MAIL & RECORDS MGMT

1 (PDF) GOVT PRINTG OFC A MALHOTRA

46 (PDF) DIR USARL
RDRL CIH C
J KNAP
L MUNDAY
X WANG
RDRL WM
B FORCH
S KARNA
J MCCAULEY
RDRL WML B
I BATYREV
B RICE
D TAYLOR
N WEINGARTEN
RDRL WML H
B AYDELOTTE
D MALLICK
C MEYER
B SCHUSTER
RDRL WMM
J BEATTY
RDRL WMM B
G GAZONAS
D HOPKINS
B LOVE
B POWERS
C RANDOW
T SANO
R WILDMAN
RDRL WMM E
J LASALVIA
J SWAB
RDRL WMM F
M TSCHOPP
RDRL WMM G
J ANDZELM
RDRL WMP
S SCHOENFELD
RDRL WMP B
C HOPPEL
S SATAPATHY
M SCHEIDLER
A SOKOLOW
T WEERASOORIYA
RDRL WMP C
R BECKER
S BILYK
T BJERKE
D CASEM
J CLAYTON
D DANDEKAR
M FERMEN-COKER
M GREENFIELD
R LEAVY
J LLOYD
S SEGLETES
A TONGE
C WILLIAMS
RDRL WMP D
R DONEY

INTENTIONALLY LEFT BLANK.